Biochemical and Biophysical Research Communications 456 (2015) 933–937

Contents lists available at ScienceDirect

Biochemical and Biophysical Research Communications

journal homepage: www.elsevier.com/locate/ybbrc

Transmitochondrial mito-miceΔ and mtDNA mutator mice, but not aged mice, share the same spectrum of musculoskeletal disorders

Takayuki Mito [a], Hikari Ishizaki [a], Michiko Suzuki [a], Hitomi Morishima [a], Azusa Ota [a], Kaori Ishikawa [a], Kazuto Nakada [a,b], Akiteru Maeno [c], Toshihiko Shiroishi [c], Jun-Ichi Hayashi [a,b,d,*]

[a] Faculty of Life and Environmental Sciences, University of Tsukuba, Tsukuba, Ibaraki, Japan
[b] International Institute for Integrative Sleep Medicine (WPI-IIIS), University of Tsukuba, Tsukuba, Ibaraki, Japan
[c] Mammalian Genetics Laboratory, National Institute of Genetics, Mishima, Shizuoka, Japan
[d] TARA Center, University of Tsukuba, Tsukuba, Ibaraki 305-8572, Japan

ARTICLE INFO

Article history:
Received 28 November 2014
Available online 12 December 2014

Keywords:
mtDNA mutator mice
Mito-miceΔ
Mitochondrial diseases
Aging
Osteoporosis
Sarcopenia

ABSTRACT

The spectra of phenotypes associated with aging and mitochondrial diseases sometimes appear to overlap with each other. We used aged mice and a mouse model of mitochondrial diseases (transmitochondrial mito-miceΔ with deleted mtDNA) to study whether premature aging phenotypes observed in mtDNA mutator mice are associated with aging or mitochondrial diseases. Here, we provide convincing evidence that all the mice examined had musculoskeletal disorders of osteoporosis and muscle atrophy, which correspond to phenotypes prevalently observed in the elderly. However, precise investigation of musculoskeletal disorders revealed that the spectra of osteoporosis and muscle atrophy phenotypes in mtDNA mutator mice were very close to those in mito-miceΔ, but different from those of aged mice. Therefore, mtDNA mutator mice and mito-miceΔ, but not aged mice, share the spectra of musculoskeletal disorders.

1. Introduction

Human mtDNA with pathogenic mutations that induce mitochondrial respiration defects has been proposed to cause mitochondrial diseases, and could also be involved in aging [1–5]. This concept (mitochondria theory of aging) is supported by studies in mtDNA mutator mice [6,7]. In these mice, proofreading-defective mtDNA polymerase enhances accumulation of somatic mtDNA mutations and leads to age-associated respiration defects and various premature aging phenotypes.

In contrast, our previous studies revealed that age-associated respiration defects found in human fibroblasts are caused not by mtDNA mutations [8,9] but by nuclear-recessive mutations [9]. Moreover, transmitochondrial mito-mice carrying mtDNA with a large-scale deletion (mito-miceΔ) showed age-associated accumulation of the mutated mtDNA and the resultant expression of phenotypes of mitochondrial diseases, but had no premature aging phenotypes [10,11]. Therefore, it appeared to be controversial that mtDNA mutator mice, but not mito-miceΔ, express premature aging phenotypes, even though both mice express age-associated respiration defects due to age-associated accumulation of mtDNA with mutations.

Our subsequent study [12] revealed that the apparent discrepancy was partly due to the differences in the nuclear genetic backgrounds of mtDNA mutator mice and mito-miceΔ: by generating mtDNA mutator mice that share the same C57BL/6J (B6J) nuclear genetic background as that of mito-miceΔ, we showed that both mouse models commonly exhibit premature aging phenotypes of kyphosis and a short lifespan, but do not express premature aging phenotypes of graying and alopecia [12]. Thus, the spectra of abnormalities in the mtDNA mutator mice with a B6J nuclear background are very similar to those of mito-miceΔ that express phenotypes of mitochondrial diseases [10,11].

The question that then arises is whether mtDNA mutator mice correspond to a model of aging or mitochondrial diseases. Here we addressed this issue by using aged mice and mito-miceΔ as positive controls for aging and mitochondrial diseases, respectively, and investigated precisely musculoskeletal disorders, including osteoporosis and muscle atrophy, which have been reported in elderly human subjects [13] and mtDNA mutator mice [6,7].

* Corresponding author at: TARA Center, University of Tsukuba, Tsukuba, Ibaraki 305-8572, Japan. Fax: +81 298 53 6614.
E-mail address: jih45@biol.tsukuba.ac.jp (J.-I. Hayashi).

http://dx.doi.org/10.1016/j.bbrc.2014.12.009
0006-291X/

2. Materials and methods

2.1. Mice

Inbred B6J mice generated by sibling mating more than 40 times were obtained from CLEA Japan. Mito-miceΔ and mtDNA mutator mice were generated in our previous studies [10,12]. Animal experiments were performed in accordance with protocols approved by the Experimental Animal Committee of the University of Tsukuba, Japan.

2.2. Micro-computed tomography analysis

The μ-CT (Scan X mate E090S scanner, Comscantechno, Kanagawa, Japan) was used to take tomography images at three parts in mouse tibia bones. The μ-CT was operated at a tube voltage peak of 90 kV and a tube current of 90 mA. Samples were rotated 360° in steps of 0.6°, generating 600 projection images of 992 × 992 pixels. The μ-CT data were reconstructed at an isotropic resolution of $22.4 \times 22.4 \times 22.4\ mm^3$ (the wide part of tibia) and $7 \times 7 \times 7\ mm^3$ (the proximal metaphysis and the mid-diaphysis). 0.1 mm brass filter was used for the scanning of the wide part of tibia and the mid-diaphysis. For each analysis, the region of interest (ROI) was defined on the basis of an anatomical feature (Fig. S1). Morphometric indices were calculated using TRI/3D-BON (RATOC System Engineering, Tokyo, Japan) software. Bone mineral density of tibia bones were measured using TRI/3D-BON-BMD (RATOC Systems) software.

2.3. Quantitative RT-PCR

Total RNA was extracted from mouse quadriceps muscles by using the RNeasy fibrous mini kit (Qiagen, Hilden, Germany). RNA samples were reverse transcribed by using QuantiTect Reverse Transcription Kit (Qiagen). Real-time monitoring PCR was performed with QuantiTect SYBR Green PCR Kit (Qiagen), an ABI PRISM 7900HT sequence detection system (Applied Biosystems, CA, USA), and primers for atrogin-1 (forward, ctctgtaccatgccgttcct; reverse, ggctgctgaacagattctcc) and TATA-box binding protein (forward, ggcggtttggctaggttt; reverse: gggttatcttcacacaccatga). The relative expression level of *atrogin*-1 mRNA was calculated by using ΔΔCt method. The gene encoding TATA-box binding protein was used as an internal control. The proportion of wild type mtDNA and ΔmtDNA was determined by real-time PCR analysis, as described previously [12].

2.4. Ex vivo differentiation of osteoclasts and osteoblasts

Bone marrow macrophages were induced by incubating bone marrow flushed from mouse femurs and tibiae with macrophage inducing medium: MEMα Glutamax (Gibco, CA, USA) containing 10% fetal bovine serum (FBS) and 10 ng/mL recombinant macrophage colony stimulating factor 1 (M-CSF) (Wako, Osaka, Japan), and purified by Ficoll-Hypaque (GE Healthcare, Buckinghamshire, UK) gradient centrifugation. Osteoclasts were induced by incubating bone marrow macrophages in MEMα Glutamax containing 10% FBS, 50 ng/mL recombinant M-CSF, and 100 ng/mL recombinant receptor activator of nuclear factor kappa-B ligand (RANKL) (Wako) for 5 days. Pre-osteoblasts were selected from bone marrow by incubating whole bone marrow cells in RPMI1640 (Nissui, Tokyo, Japan) containing 10% FBS for 7 days. Osteoblasts were induced by incubating pre-osteoblasts in RPMI1640 containing Osteoblast-Inducer Reagent (TaKaRa, Shiga, Japan) for 14 days. Cytochemical analysis of cytochrome *c* oxidase (COX) activity of osteoclasts and osteoblasts was performed as described previously [12].

2.5. Histological analyses

Frozen sections (10-μm) of quadriceps muscles were used for COX and H&E staining, as described previously [12]. Cross sectional area (CSA) of skeletal muscle fibers was calculated from H&E stained section by using ImageJ (Rasband, WS., Image J, U.S. National Institutes of Health, Bethesda, Maryland, USA, http://imagej.nih.gov/ij/, 1997–2014) software.

2.6. Statistical analysis

Data were analyzed by two-sided Student's *t*-test. *P* values of less than 0.05 were considered significant.

3. Results

First we compared bone mineral density (BMD) in aged mice, mtDNA mutator mice, and mito-miceΔ, because decreased BMD is an osteoporosis phenotype prevalent in elderly human subjects and a phenotype observed in mtDNA mutator mice. We carried out quantitative estimation of BMD in tibia bones (Fig. S1A), and showed that its expression was significantly decreased in aged mice, mtDNA mutator mice, and mito-miceΔ compared with young mice (Fig. 1A).

For further investigation of the structural abnormalities associated with the decreased BMD (Fig. 1B), we performed X-ray micro-computed tomography (μ-CT) analysis of trabecular and cortical bones (Fig. S1B and C). Quantitative estimation of trabecular bone volume (Fig. 1C) and cortical bone thickness (Fig. 1D) showed that cortical bone thickness, but not trabecular bone volume, decreased in both mtDNA mutator mice and mito-miceΔ; in contrast, aged mice did not show a significant decrease in either trabecular bone volume or cortical bone thickness. Together with the finding that elderly human subjects exhibit a decrease in trabecular bone volume but not cortical bone thickness [14], our result suggests that decreased cortical bone thickness exclusively found in mtDNA mutator mice and mito-miceΔ is not associated with either mouse or human aging.

We then compared respiratory function by using osteoclasts and osteoblasts, which play an important role in bone metabolism. Cytochemical analysis of mitochondrial cytochrome *c* oxidase (COX) activity showed reduced activity in the cells of mtDNA mutator mice and mito-miceΔ, but not in the cells of aged mice, when compared with young mice (Fig. 1E). These results indicate that the decreased BMD (Fig. 1A) and cortical bone thickness (Fig. 1D) observed in mtDNA mutator mice and mito-miceΔ are likely due to respiration defects, whereas the decreased BMD observed in aged mice (Fig. 1A) occurred in the absence of the respiration defects (Fig. 1E).

Next, we investigated muscle atrophy, another typical aging phenotype of musculoskeletal disorders, which is observed not only in elderly human subjects [13] and mtDNA mutator mice [6,7], but also in patients with mitochondrial diseases [15], cachexia, or sepsis [16]. By isolating and measuring the weight of quadriceps muscles (Fig. 2A and B), we observed muscle atrophy in aged mice, mtDNA mutator mice, and mito-miceΔ compared with young mice. Furthermore, histochemical analysis also showed atrophy of each muscle fiber (Fig. 2C and D), which confirmed the presence of muscle atrophy in the quadriceps of all three mouse models.

Comparison of the mitochondrial respiratory function of quadriceps was performed by histochemical analysis of COX activity.

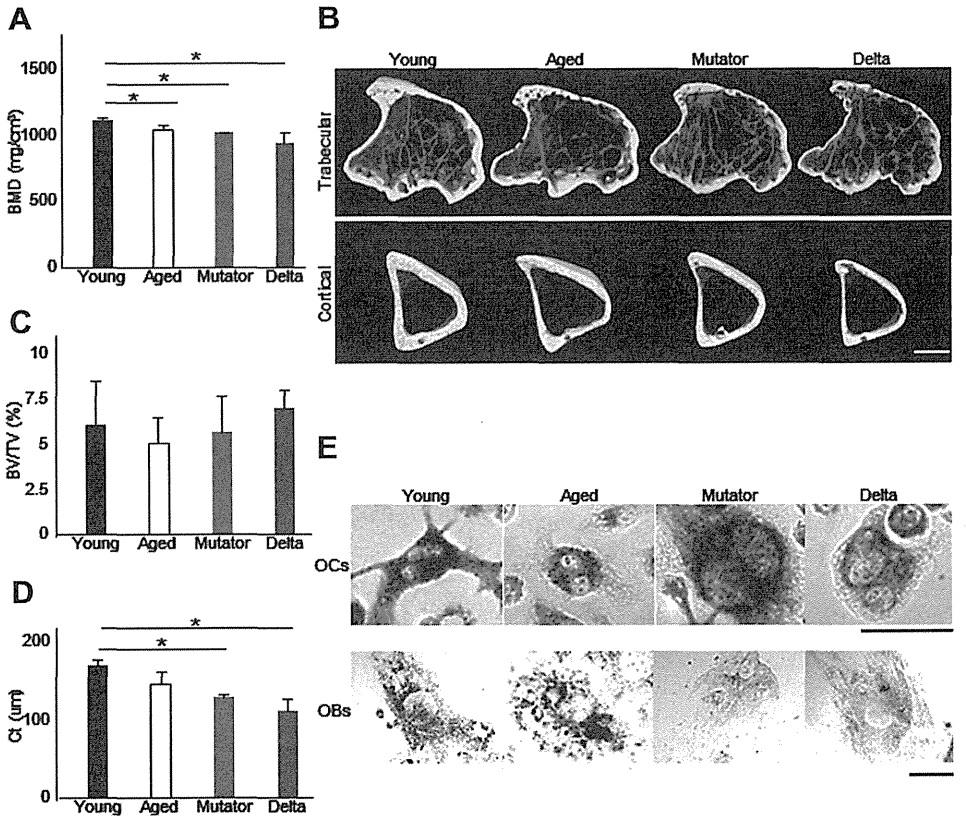

Fig. 1. Characterization of phenotypes of osteoporosis displayed in tibia bones of mtDNA mutator mice. Aged mice and mito-miceΔ were used as controls expressing phenotypes associated with aging and mitochondrial diseases, respectively. All mice were males sharing the B6J nuclear genetic background. Young, 10-month-old mice; Aged, 27-month-old mice; Mutator, 10-month-old mtDNA mutator mice; Delta, 10-month-old mito-miceΔ. The proportions of ΔmtDNA in the tail from mito-miceΔ were 57.5 ± 2.5% at 4 weeks after birth and 81.2 ± 1.3% at 10 months old. (A) Quantitative estimation of BMD. Data are means ± SD. $^*P < 0.05$ ($n = 3$). (B) μ-CT analysis of trabecular and cortical bones. Upper panel, red-colored areas correspond to trabecular bones; lower panel, bone areas exclusively consisting of cortical bones (gray-colored areas). Scale bar, 500 μm. (C) Quantitative estimation of the ratio of trabecular bone volume/tissue volume (BV/TV). Data are means ± SD. $^*P < 0.05$ ($n = 3$). (D) Quantitative estimation of cortical bone thickness (Ct). Data are means ± SD. $^*P < 0.05$ ($n = 3$). (E) Cytochemical analysis of COX activity. OCs, osteoclasts; OBs, osteoblasts. Cells that had lost their COX activity were detected as a blue color. The proportions of ΔmtDNA in the bone marrow cells, osteoclasts, and osteoblasts were 65.1%, 61.5%, and 57.7%, respectively. Scale bars, 50 μm.

Decreased COX activity relative to that in young mice was observed in muscle fibers of mtDNA mutator mice and mito-miceΔ, but not in aged mice (Fig. 2E). Therefore, mitochondrial respiration defects could be responsible for the muscle atrophy expressed in mtDNA mutator mice and mito-miceΔ, whereas aged mice had muscle atrophy in the absence of the respiration defects. Decreased COX activity in muscle fibers corresponds to mitochondrial myopathy, which is one of the typical abnormalities frequently observed in patients with mitochondrial diseases [1,4]. Therefore, mtDNA mutator mice and mito-miceΔ also share a phenotype associated with mitochondrial diseases.

For further investigation of muscle atrophy, we examined *atrogin*-1 mRNA levels, because overexpression of the *atrogin*-1 gene, which encodes an E3 ubiquitin ligase involved in proteolysis, is observed in human muscle atrophy caused by cachexia, sepsis, or immobilization [16], but not in age-associated muscle atrophy (sarcopenia) developed in the elderly [17]. Here we observed that *atrogin*-1 mRNA was overexpressed in quadriceps of both mtDNA mutator mice and mito-miceΔ, but not in aged mice, relative to the levels in young mice (Fig. 2F). These observations suggest that the mechanisms behind muscle atrophy in mtDNA mutator mice are similar to those in mito-miceΔ, but differ from those in aged mice and elderly human subjects, that develop muscle atrophy in the absence of *atrogin*-1 overexpression.

4. Discussion

The mitochondrial theory of aging [1–5] proposes a vicious cycle of age-associated accumulation of somatic mutations in mtDNA and the resultant respiration defects and overproduction of reactive oxygen species (ROS). This concept was partly supported by studies in mtDNA mutator mice, which had premature aging phenotypes along with the accumulation of somatic mutations in mtDNA, although they did not display ROS overproduction [7,18]. However, mito-miceΔ showing age-associated accumulation of the mutated mtDNA and the resultant respiration defects had no premature aging phenotypes [10,11]. We addressed to the controversial issue that mtDNA mutator mice, but not mito-miceΔ, express premature aging phenotypes, and revealed that decreased cortical bone thickness (Fig. 1D) and overexpression of *atrogin*-1 in muscle atrophy (Fig. 2F) were exclusively observed in mtDNA mutator mice and mito-miceΔ, but not in aged mice.

Therefore, the spectra of musculoskeletal disorders in mtDNA mutator mice and mito-miceΔ are similar to each other, but different from those in aged mice. Considering that the spectra of musculoskeletal disorders in mtDNA mutator mice and mito-miceΔ are also different from those in elderly human subjects [14,17], they would not be associated with either mouse or human aging. Then, a question that arises is whether decreased cortical bone thickness and increased *atrogin*-1 mRNA expression in muscle fibers are

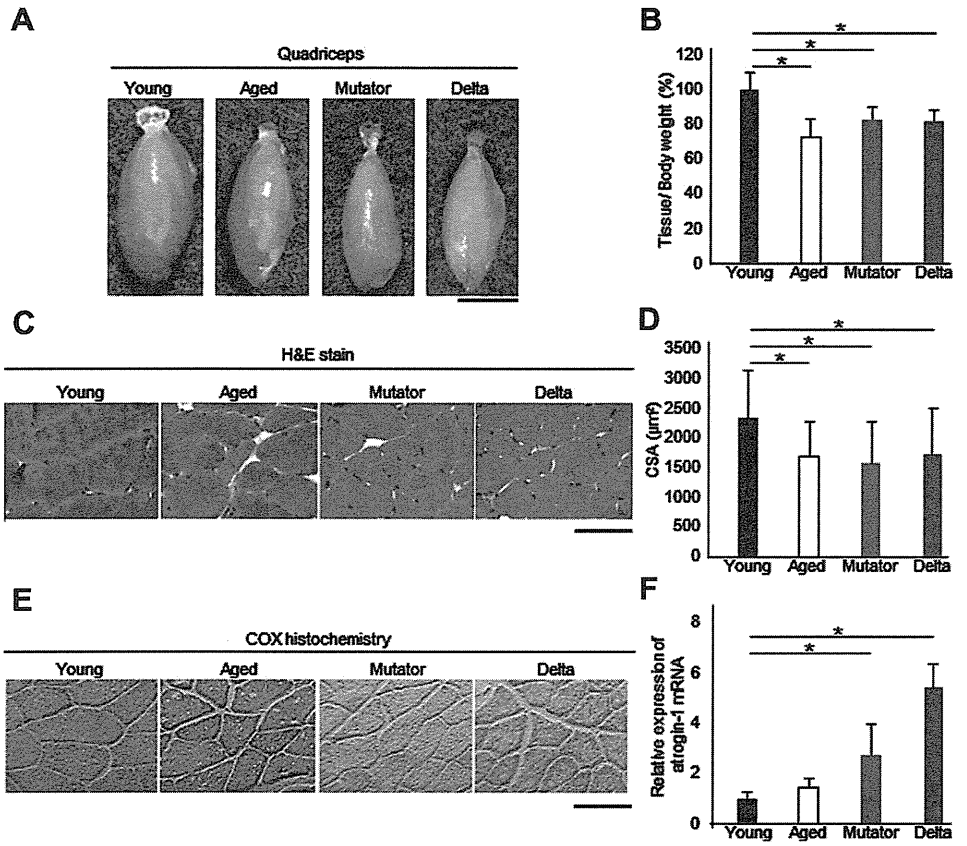

Fig. 2. Characterization of phenotypes of muscle atrophy displayed in quadriceps of mtDNA mutator mice. Aged mice and mito-miceΔ were used as controls of phenotypes associated with aging and mitochondrial disease, respectively. All mice were males sharing the B6J nuclear genetic background. Young, 10-month-old mice; Aged, 27-month-old mice; Mutator, 10-month-old mtDNA mutator mice; Delta, 10-month-old mito-miceΔ. (A) Images of whole quadriceps. The proportions of ΔmtDNA in the quadriceps from mito-miceΔ were 82.6%. Scale bar, 5 mm. (B) Tissue weights of quadriceps. The proportions of ΔmtDNA in the quadriceps muscles from mito-miceΔ were 83.1 ± 2.2%. Data are means ± SD. $^*P < 0.05$ ($n = 3$). (C) Hematoxylin and eosin (H&E) staining of muscle fibers in quadriceps. The proportions of ΔmtDNA in the quadriceps from mito-miceΔ were 83.2%. Scale bar, 50 μm. (D) Quantitative estimation of cross-sectional areas (CSA) of each muscle fiber. The proportions of ΔmtDNA in the quadriceps muscles from mito-miceΔ were 82.9 ± 2.1%. Data are means ± SD. $^*P < 0.05$. (E) Histochemical analysis of COX activity in quadriceps. The intensity of brown-staining represents the level of COX activity. The proportions of ΔmtDNA in the quadriceps from mito-miceΔ were 82.7%. Scale bar, 50 μm. (F) Estimation of the mRNA levels of *atrogin*-1 in quadriceps by using quantitative real-time PCR. The proportions of ΔmtDNA in the quadriceps muscles from mito-miceΔ were 83.0 ± 1.8%. Data are means ± SD. $^*P < 0.05$ ($n = 4$).

associated with mitochondrial diseases. To answer this question, further works are required to investigate whether the patients with mitochondrial diseases express these abnormalities.

Conflict of interest

The authors have no conflict of interest.

Acknowledgments

This work was supported by Grants-in-Aid for Scientific Research (A) (No. 23240058 and No. 25250011) from the Ministry of Education, Culture, Sports, Science and Technology of Japan (MEXT) to K.N. and J.I.H., respectively. This work was also supported by a Grant-in-Aid for Japan Society for the Promotion of Science (JSPS) Fellows (No. 26-467) to T.M.

Appendix A. Supplementary data

Supplementary data associated with this article can be found, in the online version, at http://dx.doi.org/10.1016/j.bbrc.2014.12.009.

References

[1] D.C. Wallace, Mitochondrial diseases in man and mouse, Science 283 (1999) 1482–1488.
[2] H.T. Jacobs, The mitochondrial theory of aging: dead or alive?, Aging Cell 2 (2003) 11–17
[3] L.A. Loeb, D.C. Wallace, G.M. Martin, The mitochondrial theory of aging and its relationship to reactive oxygen species damage and somatic mtDNA mutations, Proc. Natl. Acad. Sci. U.S.A. 102 (2005) 18769–18770.
[4] R.W. Taylor, D.M. Turnbull, Mitochondrial DNA mutations in human disease, Nat. Rev. Genet. 6 (2005) 389–402.
[5] K. Khrapko, J. Vija, Mitochondrial DNA mutations and aging: devils in the details?, Trends Genet 25 (2009) 91–98.
[6] A. Trifunovic, A. Wredenberg, M. Falkenberg, J.N. Spelbrink, A.T. Rovio, C.E. Bruder, Y.M. Bohlooly, S. Gidlof, A. Oldfors, R. Wibom, J. Tornell, H.T. Jacobs, N.G. Larsson, Premature ageing in mice expressing defective mitochondrial DNA polymerase, Nature 429 (2004) 417–423.
[7] G.C. Kujoth, A. Hiona, T.D. Pugh, S. Someya, K. Panzer, S.E. Wohlgemuth, T. Hofer, A.Y. Seo, R. Sullivan, W.A. Jobling, J.D. Morrow, H. Van Remmen, J.M. Sedivy, T. Yamasoba, M. Tanokura, R. Weindruch, C. Leeuwenburgh, T.A. Prolla, Mitochondrial DNA mutations, oxidative stress, and apoptosis in mammalian aging, Science 309 (2005) 481–484.
[8] J.-I. Hayashi, S. Ohta, Y. Kagawa, H. Kondo, H. Kaneda, H. Yonekawa, D. Takai, S. Miyabayashi, Nuclear but not mitochondrial genome involvement in human age-related mitochondrial dysfunction, J. Biol. Chem. 269 (1994) 6878.
[9] K. Isobe, S. Ito, H. Hosaka, Y. Iwamura, H. Kondo, Y. Kagawa, J.-I. Hayashi, Nuclear-recessive mutations of factors involved in mitochondrial translation are responsible for age-related respiration deficiency of human skin fibroblasts, J. Biol. Chem. 273 (1998) 4601.
[10] K. Inoue, K. Nakada, A. Ogura, K. Isobe, Y.-I. Goto, I. Nonaka, J.-I. Hayashi, Generation of mice with mitochondrial dysfunction by introducing mouse mtDNA carrying a deletion into zygotes, Nat. Genet. 26 (2000) 176–181.

[11] K. Nakada, K. Inoue, T. Ono, K. Isobe, A. Ogura, Y.-I. Goto, I. Nonaka, J.-I. Hayashi, Inter-mitochondrial complementation: mitochondria-specific system preventing mice from expression of disease phenotypes by mutant mtDNA, Nat. Med. 7 (2001) 934–940.
[12] T. Mito, Y. Kikkawa, A. Shimizu, O. Hashizume, S. Katada, H. Imanishi, A. Ota, Y. Kato, K. Nakada, J.-I. Hayashi, Mitochondrial DNA mutations in mutator mice confer respiration defects and B-cell lymphoma development, PLoS ONE 8 (2013) e55789.
[13] A. Nedergaard, K. Henriksen, M.A. Karsdal, C. Christiansen, Musculoskeletal ageing and primary prevention, Best Pract. Res. Clin. Obstet. Gynaecol. 27 (2013) 678–688.
[14] A.E. Rosenberg, The pathology of metabolic bone disease, Radiol. Clin. North Am. 29 (1991) 19–36.
[15] B.H. Cohen, Neuromuscular and systemic presentations in adults: diagnoses beyond MERRF and MELAS, Neurotherapeutics 10 (2013) 227–242.
[16] V.C. Foletta, L.J. White, A.E. Larsen, B. Leger, A.P. Russell, The role and regulation of MAFbx/atrogin-1 and MuRF1 in skeletal muscle atrophy, Pflugers Arch. 461 (2011) 325–335.
[17] K. Sakuma, W. Aoi, A. Yamaguchi, The intriguing regulator of muscle mass in sarcopenia and muscular dystrophy, Front. Aging Neurosci. 6 (2014) 230.
[18] A. Trifunovic, A. Hansson, A. Wredenberg, A.T. Rovio, E. Dufour, I. Khvorostov, J.N. Spelbrink, R. Wibom, H.T. Jacobs, N.G. Larsson, Somatic mtDNA mutations cause aging phenotypes without affecting reactive oxygen species production, Proc. Natl. Acad. Sci. U.S.A. 102 (2005) 17993–17998.

Biochemical and Biophysical Research Communications 459 (2015) 66–70

Contents lists available at ScienceDirect

Biochemical and Biophysical Research Communications

journal homepage: www.elsevier.com/locate/ybbrc

G7731A mutation in mouse mitochondrial $tRNA^{Lys}$ regulates late-onset disorders in transmitochondrial mice

Akinori Shimizu [a], Takayuki Mito [a], Osamu Hashizume [a], Hiromichi Yonekawa [b], Kaori Ishikawa [a], Kazuto Nakada [a, c], Jun-Ichi Hayashi [a, c, d, *]

[a] Faculty of Life and Environmental Sciences, University of Tsukuba, 1-1-1 Tennodai, Tsukuba, Ibaraki, 305-8572, Japan
[b] Department of Laboratory Animal Science, The Tokyo Metropolitan Institute of Medical Science, 2-1-6 Kamikitazawa, Setagaya-ku, Tokyo, 156-8506, Japan
[c] International Institute for Integrative Sleep Medicine (WPI-IIIS), University of Tsukuba, 1-1-1 Tennodai, Tsukuba, Ibaraki, 305-8572, Japan
[d] TARA Center, University of Tsukuba, 1-1-1 Tennodai, Tsukuba, Ibaraki, 305-8572, Japan

ARTICLE INFO

Article history:
Received 6 February 2015
Available online 23 February 2015

Keywords:
G7731A mtDNA mutation
Mitochondrial $tRNA^{Lys}$ gene
Transmitochondrial mice
Respiration defects
Late-onset disorders
Mitochondrial disease models

ABSTRACT

We previously generated mito-mice-$tRNA^{Lys7731}$ as a model for primary prevention of mitochondrial diseases. These mice harbour a G7731A mtDNA mutation in the $tRNA^{Lys}$ gene, but express only muscle weakness and short body length by four months. Here, we examined the effects of their aging on metabolic and histologic features. Unlike young mito-mice-$tRNA^{Lys7731}$, aged mito-mice-$tRNA^{Lys7731}$ developed muscle atrophy, renal failures, and various metabolic abnormalities, such as lactic acidosis and anemia, characteristic of patients with mitochondrial diseases. These observations provide convincing evidence that the respiration defects induced by high G7731A mtDNA levels cause these late-onset disorders that are relevant to mitochondrial diseases.

1. Introduction

The accumulation of mitochondrial DNA (mtDNA) with pathogenic mutations is proposed to be closely associated with mitochondrial diseases, normal aging, and age-associated disorders, including diabetes, because of its induction of significant respiration defects [1–3]. Three most prevalent mitochondrial diseases are chronic progressive external ophthalmoplegia (CPEO), due to mtDNA with large-scale deletions (ΔmtDNA); myoclonic epilepsy with ragged-red fibers (MERRF), due to single-point mutations in the $tRNA^{Lys}$ gene; and mitochondrial myopathy, encephalopathy, lactic acidosis, and stroke-like episodes syndrome (MELAS), due to single-point mutations in the $tRNA^{Leu(UUR)}$ gene [1–3]. Subsequent studies [4–6] have proved the pathogenicities of these mtDNA mutations by inducing respiration defects after the transfer of patient-derived mutated mtDNA into mtDNA-less human cells. However, it has not been established unequivocally whether the respiration defects due to the accumulation of mtDNA with pathogenic mutations in the tissues actually induce the various clinical phenotypes observed in patients with mitochondrial diseases or with age-associated disorders.

This issue was resolved in part by our previous studies [7–11], in which we generated transmitochondrial mice (mito-mice) carrying exogenously introduced mouse mtDNA with mutations orthologous to those found in patients with mitochondrial diseases. For example, mito-mice-Δ, which harbored mouse ΔmtDNA and therefore corresponded to disease models for CPEO, simultaneously expressed respiration defects, which were induced by accumulated ΔmtDNA, and disease phenotypes corresponding to those of CPEO in humans [7,8]. Therefore, experiments in mito-mice could provide convincing evidence that the respiration defects due to mtDNA mutations regulate clinical abnormalities relevant to mitochondrial diseases or age-associated disorders.

We recently generated mito-mice-$tRNA^{Lys7731}$, which harbour mtDNA that contain a pathogenic G7731A mutation in the $tRNA^{Lys}$ gene (G7731A mtDNA), as a model for primary prevention of mitochondrial diseases [12]. Because a G8328A mutation orthologous to the mouse G7731A mutation occurs in patients with mitochondrial diseases [13,14], mito-mice-$tRNA^{Lys7731}$ can be used

Abbreviations: mtDNA, mitochondrial DNA; ΔmtDNA, mtDNA with large-scale deletions; CPEO, chronic progressive external ophthalmoplegia; MERRF, myoclonic epilepsy with ragged red fibers; MELAS, mitochondrial myopathy, encephalopathy, lactic acidosis, and stroke-like episodes syndrome; COX, cytochrome c oxidase; RRFs, ragged red fibers; SDH, succinate dehydrogenase.

* Corresponding author. TARA Center, University of Tsukuba, 1-1-1 Tennodai, Tsukuba, Ibaraki, 305-8572, Japan. Fax: +81 298536650.
E-mail address: jih45@biol.tsukuba.ac.jp (J.-I. Hayashi).

http://dx.doi.org/10.1016/j.bbrc.2015.02.070
0006-291X/

as prospective models for diseases that, like MERRF, are caused by mutations in the mitochondrial *tRNA^{Lys}* gene. Young mito-mice-tRNA^{Lys7731} with high levels of G7731A mtDNA expressed respiration defects and the resultant phenotypic features characteristic of mitochondrial diseases, such as short body length and muscle weakness, but they did not exhibit ragged red fibers (RRFs) or other traits seen in patients with mitochondrial diseases [12].

Here, to compare the effects of aging on the expression of phenotypes characteristic of mitochondrial diseases and age-associated disorders, we used aged mito-mice-tRNA^{Lys7731} that share the same nuclear background but carry either low or high levels of G7731A mtDNA.

2. Materials and methods

Mice. Inbred B6 mice were obtained from CLEA Japan. Mito-mice-tRNA^{Lys7731} were generated in our previous work [12]. Animal experiments were performed in accordance with protocols approved by the Experimental Animal Committee of the University of Tsukuba, Japan (approval number, 14243).

Genotyping of mtDNA. To detect the G7731A mutation, a 130-bp fragment containing the 7731 site was PCR-amplified by using the nucleotide sequences from 7633 to 7653 (5′-GCCCATTGTCCT AGAAATGGT-3′) and 7762 to 7732 (5′-ACTATGGAGATTTTAAGG TCTCTAACTTTAA-3′) as oligonucleotide primers. The G7731A mutation creates a restriction site for *DraI* and generates 96- and 34-bp fragments on DraI digestion of PCR products. The restriction fragments were separated by electrophoresis in a 3% agarose gel. For quantification of G7731A mtDNA, we used ImageJ (Rasband, WS., Image J, U.S. National Institutes of Health, Bethesda, Maryland, USA, http://imagej.nih.gov/ij/, 1997–2014) software.

Histopathologic analyses. Formalin-fixed, paraffin-embedded sections (thickness, 5 μm) were stained with hematoxylin and eosin (H&E) to identify features characteristic of renal failures. Cryosections (thickness, 10 μm) of skeletal muscle were stained with modified Gomori trichrome for histopathologic analysis to identify RRFs. Cryosections (thickness, 10 μm) of renal tissues were prepared, and histologic analyses of COX and succinate dehydrogenase activities were performed as described previously [15].

Grip strength test. Muscle strength was estimated by using a Grip Strength Meter (Columbus Instruments, Columbus, USA); three sequential trials were performed on each mouse bilaterally.

Measurement of blood glucose, lactate, and BUN. To determine fasting blood lactate and glucose concentrations, peripheral blood was collected from the tail veins of mice after food had been withheld overnight. Glucose (1.5 g/kg body weight) was administered orally, blood was collected 15–120 min after glucose administration, and lactate and glucose concentrations were measured with an automatic blood lactate meter (Lactate Pro 2; Arkray, Kyoto, Japan) and glucose meter (Dexter ZII; Bayer, Leverkusen, Germany), respectively. BUN was measured with a Urea N B test (Wako Pure Chemical, Osaka, Japan) in accordance with the manufacturer's protocol.

Measurement of hematocrit. To determine hematocrit, capillary blood samples were obtained from each mouse by using heparinized capillary tubes, which then were centrifuged at 10,500 × *g* for 5 min. Packed cell volumes were measured by using a hematocrit reader.

Statistical analysis. Data are presented as mean ± SD and were analysed by using Student's *t* test; *P* values less than 0.05 were considered significant. Excel software was used for all statistical analysis.

3. Results

3.1. Late-onset metabolic abnormalities in aged mito-mice-tRNA^{Lys7731}

We used aged (26-month-old) male mito-mice-tRNA^{Lys7731} with low (<5%) or high (70%–75%) levels of G7731A mtDNA in their tails at 4 weeks after birth and age- and sex-matched B6 mice (negative controls). We first evaluated body length (Fig. 1A) and muscle strength (Fig. 1B), because abnormalities in these phenotypes are expressed in young (4-month-old) mito-mice-tRNA^{Lys7731} [12] and can be examined without killing the mice. Short body length (Fig. 1A) and muscle weakness (Fig. 1B), which are closely associated with the clinical abnormalities caused by the orthologous G8328A mutation in the human mitochondrial *tRNA^{Lys}* gene [13,14], occurred exclusively in mito-mice-tRNA^{Lys7731} with high levels of G7731A mtDNA. These results are consistent with our previous findings obtained from young mito-mice-tRNA^{Lys7731} [12].

We then examined various metabolic parameters relevant to mitochondrial diseases. Whereas these features were normal in our young mito-mice-tRNA^{Lys7731} [12], we expected that abnormalities in these parameters would be expressed as late-onset disorders as the mito-mice-tRNA^{Lys7731} aged. Unlike aged B6 mice and aged mito-mice-tRNA^{Lys7731} with low levels of G7731A mtDNA, aged mito-mice-tRNA^{Lys7731} with high levels of G7731A mtDNA exclusively had low hematocrit values (Fig. 1C), lactic acidosis (Fig. 1D),

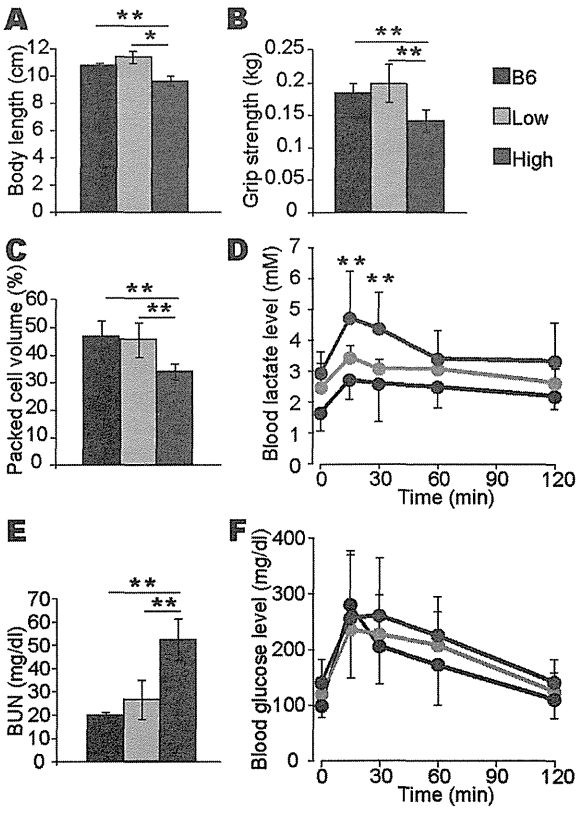

Fig. 1. Mitochondrial disease–related parameters that can be examined without euthanizing aged mito-mice-tRNA^{Lys7731}. Study populations comprised aged B6 mice ($n = 6$) and aged mito-mice-tRNA^{Lys7731} with low (less than 5% in tail tissue; $n = 4$) and high ($n = 4$; 70%, 70%, 72%, and 75% in tail tissue [Fig. S1]) levels of G7731A mtDNA in tails at 4 weeks after birth. Disease-related parameters were compared at 26 months after birth. Intergroup comparison of (A) body length, (B) grip strength, (C) hematocrit, (D) blood lactate level, (E) BUN value, and (F) blood glucose level. Data are presented as means ± 1 SD. *, $P < 0.05$; **, $P < 0.01$.

and increased levels of BUN in the peripheral blood (Fig. 1E). In contrast, although patients with mitochondrial diseases sometimes demonstrate mitochondrial diabetes [1–3], neither group of aged mito-mice-tRNA^{Lys7731} manifested hyperglycemia (Fig. 1F). Therefore, except for hyperglycemia, the metabolic abnormalities seen in patients with mitochondrial diseases were expressed as late-onset disorders in aged mito-mice-tRNA^{Lys7731} with high levels of G7731A mtDNA.

3.2. *Lifespan and tissue abnormalities in euthanized moribund mito-mice-tRNA^{Lys7731}*

We then assessed the lifespans of mito-mice-tRNA^{Lys7731} and the tissue abnormalities in euthanized moribund mice. The median survival times in B6 mice and in mito-mice-tRNA^{Lys7731} with low or high levels of G7731A mtDNA were 26, 28, and 27 months, respectively (Fig. 2). Thus, median survival times did not differ significantly between mito-mice-tRNA^{Lys7731} with high and low levels of G7731A mtDNA.

Gross necropsy of euthanized moribund mice showed that muscle atrophy (Fig. 3A) and anemic kidneys (Fig. 4A) occurred exclusively in mito-mice-tRNA^{Lys7731} with high levels of G7731A mtDNA. Muscle atrophy occurs not only in elderly men and women [16] and patients with mitochondrial diseases [17] but also in mtDNA mutator mice [18,19] and mito-mice-Δ that express significant respiration defects [20]. Moreover, renal abnormalities have been reported to occur occasionally in patients with mitochondrial diseases [21–23] and in mito-mice-Δ that express significant respiration defects [7,8].

We then histologically analyzed these tissues to characterize the macroscopic abnormalities in greater detail. First, we used modified Gomori trichrome staining to reveal RRFs that occur frequently in patients with mitochondrial diseases [2]. However, even aged mito-mice-tRNA^{Lys7731} with high levels of G7731A mtDNA lacked RRFs in skeletal muscle (Fig. 3B); this was consistent with our recent findings in mtDNA mutator mice and mito-mice-Δ [20].

Although the skeletal muscle was histologically normal, the anemic kidneys demonstrated multiple abnormalities. The renal cortical tubules of aged mito-mice-tRNA^{Lys7731} with high levels of G7731A mtDNA were dilated and contained casts; these changes, indicative of renal failures, did not occur in aged B6 mice or in aged mito-mice-tRNA^{Lys7731} with low levels of mutated mtDNA (Fig. 4B). Given that young mito-mice-tRNA^{Lys7731} lacked similar renal changes [12], these changes correspond to a late-onset disorder. Histologic analysis of mitochondrial respiratory function revealed decreased mitochondrial cytochrome c oxidase (COX) activity in

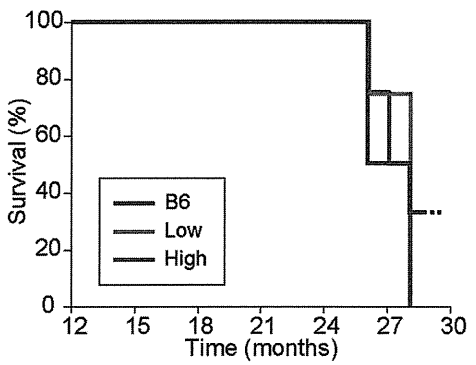

Fig. 2. Kaplan–Meier survival curves of B6 mice (n = 6) and mito-mice-tRNA^{Lys7731} with low (less than 5%; n = 4) and high (70%–75%; n = 4) levels of G7731A mtDNA. Median survival times were 26 months for B6 mice, 28 months for mito-mice-tRNA-^{Lys7731} with low levels, and 27 months for mito-mice-tRNA^{Lys7731} with high levels.

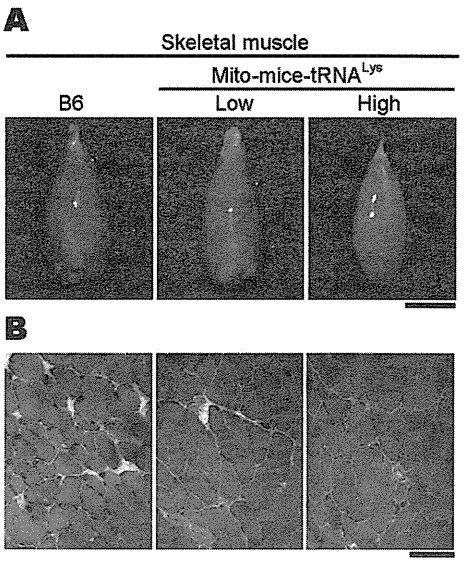

Fig. 3. Skeletal muscle abnormalities in aged mito-mice-tRNA^{Lys7731}. (A) Macroscopic evidence of muscle atrophy in the quadriceps of mito-mice-tRNA^{Lys7731} with high levels of G7731A mtDNA. Scale bar, 5 mm. (B) Histopathologic analysis of skeletal muscles to identify RRFs. Cryosections (thickness, 10 μm) of soleus muscle fibers were stained by using modified Gomori trichrome to identify RRFs. No RRFs were present even in aged mito-mice-tRNA^{Lys7731} with high levels of G7731A mtDNA. Scale bar, 50 μm. Genotyping of skeletal muscle (soleus) showed that the sample from the low group contained 5% G7731A mtDNA, whereas the sample from the high group contained 65% G7731A mtDNA.

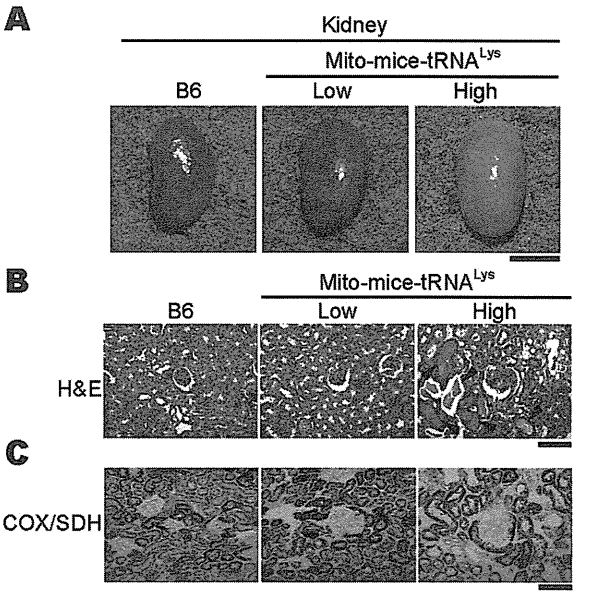

Fig. 4. Renal abnormalities in aged mito-mice-tRNA^{Lys7731}. (A) Macroscopic evidence of anemic kidneys in mito-mice-tRNA^{Lys7731} with high levels of G7731A mtDNA. (B) Hemotoxylin and eosin (H&E) staining of formalin-fixed, paraffin-embedded sections (thickness, 5 μm) of renal cortex revealed dilated lumens of renal tubules and casts (arrowheads) in mito-mice-tRNA^{Lys7731} with high levels of G7731A mtDNA. Scale bar, 50 μm. (C) Histochemical analysis of mitochondrial respiratory enzyme activities in the kidney. Tissue sections were stained for COX (brown) and succinate dehydrogenase (SDH) (blue). Cells that had lost COX activity were blue because of the absence of COX activity. Scale bar, 50 μm. Genotyping of kidney tissue showed that the sample from the low group contained 10% G7731A mtDNA, whereas the sample from the high group contained 62% G7731A mtDNA.

the kidney tissue of aged mito-mice-tRNA^{Lys7731} with high levels of G7731A mtDNA (Fig. 4C). Therefore, the respiration defects in mito-mice-tRNA^{Lys7731} with high levels of G7731A mtDNA (Fig. 4C) likely caused their renal failures (Fig. 4B).

3.3. Genotyping of G7731A mtDNA in tissues of mito-mice-tRNA^{Lys7731}

For the purposes of this study, we classified 4-week-old mito-mice-tRNA^{Lys7731} as having low or high amounts of mutated mtDNA by estimating the proportions of G7731A mtDNA isolated from samples of tail tissue. The question that then arises is whether the proportions of G7731A mtDNA differ among tissues or with age.

We estimated G7731A mtDNA proportions in various tissues of euthanized moribund mito-mice-tRNA^{Lys7731}. The results showed that, regardless of whether the mouse was characterized as having low or high amounts of mutated mtDNA, the proportion of G7731A mtDNA in the tail tissue did not differ substantially between samples obtained from the same mito-mouse-tRNA^{Lys7731} at 4 weeks compared with at 26–28 months after birth (Fig. S1). Moreover, G7731A mtDNA levels were similar among all tissue samples from the same individual mito-mice-tRNA^{Lys7731} (Fig. S1).

4. Discussion

Using mito-mice-tRNA^{Lys7731}, we showed that high levels of G7731A mtDNA and the resultant respiration defects did not affect median survival times (Fig. 2), even though they induced the late-onset disorders (Figs. 1, 3 and 4). In contrast, accumulation of pathogenic mutations in human mtDNA and the resultant respiration defects have been proposed to be responsible for features of normal aging as well as of mitochondrial diseases [1–3]. However, our current observations suggest that mtDNA with pathogenic mutations is not necessarily associated with aging processes. This idea is further supported by our previous findings that mito-mice-COI^{6589}, which contain mtDNA with a T6589C mutation in *COI*, and mito-mice-ND6^{13997}, which carry mtDNA with a G13997A mutation in *ND6*, had normal lifespans [11].

In contrast, our mito-mice-tRNA^{Lys7731} developed several phenotypes relevant to mitochondrial diseases, including anemia (Fig. 1C), lactic acidosis (Fig. 1D), and increased BUN (Fig. 1E). Moreover, euthanized moribund mito-mice-tRNA^{Lys7731} showed muscle atrophy (Fig. 3A) and renal failures (Fig. 4). The muscle atrophy in aged mito-mice-tRNA^{Lys7731} with high levels of G7731A mtDNA (Fig. 3A) likely is associated with their muscle weakness (Fig. 1B). It is also likely that the anemic kidney tissue in the aged mito-mice-tRNA^{Lys7731} (Fig. 4A) reflects their low hematocrit levels (Fig. 1C). Moreover, the increased BUN values (Fig. 1E) likely reflect the renal failures (Fig. 4B) caused by high levels of G7731A mtDNA and the resultant respiration defects (Fig. 4C). Given that mito-mice-tRNA^{Lys7731} with low and high levels of G7731A mtDNA have the same B6 nuclear genetic background, the respiration defects induced exclusively by the high levels of G7731A mtDNA are responsible for the development of these late-onset disorders.

A question that then arises is why these abnormalities have a late onset in mito-mice-tRNA^{Lys7731}, even though aging did not affect the proportions of G7731A mtDNA in the tissues (Fig. S1). One explanation is the requirement of long-term exposure of the tissues to respiration defects or the requirement of age-dependent development of nuclear abnormalities for the onset of these disorders. It is also likely that each cell in a tissue eventually contains solely mtDNA either with or without the G7731A mutation as a consequence of stochastic segregation over time [24–26], resulting in the induction of the late-onset disorders due to the apoptosis or substantial dysfunction of cells containing only G7731A mtDNA.

In contrast to their other clinically characteristic features, aged mito-mice-tRNA^{Lys7731} with high levels of G7731A mtDNA did not demonstrate peripheral hyperglycemia (Fig. 1F) indicative of mitochondrial diabetes; this disorder has been proposed to occur frequently in patients with mitochondrial diseases [1–3]. However, our results are consistent with our previous findings in mito-mice-COI^{6589}, which have normal blood glucose levels (9). In addition, blood glucose levels were low in mito-mice-Δ [27] but high in mito-mice-ND6^{13997} [11], indicating that high levels of pathogenic mtDNA mutations and the resultant respiration defects do not necessarily cause mitochondrial diabetes.

Current study also showed that all groups of our mice—even aged mito-mice-tRNA^{Lys7731} with high levels of G7731A mtDNA (that is, 70%–75%)—lacked RRFs (Fig. 3B). The absence of RRFs may be due in part to the fact that the amount of G7731A mtDNA was insufficient to induce RRFs. Thus, somehow mito-mice-tRNA^{Lys7731} with more than 75% G7731A mtDNA have to be generated for RRF development. However, the death of B6 mouse oocytes that carry levels of G7731A mtDNA in excess of 85% [12] would prevent the generation of mito-mice-tRNA^{Lys7731} with sufficient proportions of G7731A mtDNA to develop RRFs. It is likely that some as-yet unknown nuclear factors in mouse strains other than B6 may allow the survival of oocytes with more than 85% G7731A mtDNA.

To evaluate this idea, we plan to replace the B6 nuclear genetic background of mito-mice-tRNA^{Lys7731} with that from other strains. This replacement may support the survival of oocytes with more than 85% G7731A mtDNA and subsequently the development of skeletal muscle RRFs and peripheral hyperglycemia in the resultant mito-mice-tRNA^{Lys7731}.

Conflict of interest

None.

Acknowledgments

This work was supported by Grants-in-Aid for Scientific Research A (no. 25250011, to J.-I.H.), Scientific Research A (no. 23240058, to K.N.), and Scientific Research on Innovative Areas (no. 24117503, to J.-I.H.) from the Japan Society for the Promotion of Science. In addition, this work was supported by the World Premier International Research Center Initiative, Ministry of Education, Culture, Sports, Science, and Technology–Japan (to K.N. and J.-I.H.).

Appendix A. Supplementary data

Supplementary data related to this article can be found at http://dx.doi.org/10.1016/j.bbrc.2015.02.070.

Transparency document

Transparency document related to this article can be found online at http://dx.doi.org/10.1016/j.bbrc.2015.02.070.

References

[1] N.-G. Larsson, D.A. Clayton, Molecular genetic aspects of human mitochondrial disorders, Annu. Rev. Genet. 29 (1995) 151–178.
[2] D.C. Wallace, Mitochondrial diseases in man and mouse, Science 283 (1999) 1482–1488.
[3] R.W. Taylor, D.M. Turnbull, Mitochondrial DNA mutations in human disease, Nat. Rev. Genet. 6 (2005) 389–402.
[4] J.-I. Hayashi, S. Ohta, A. Kikuchi, et al., Introduction of disease-related mitochondrial DNA deletions into HeLa cells lacking mitochondrial DNA results in mitochondrial dysfunction, Proc. Natl. Acad. Sci. U. S. A. 88 (1991) 10614–10618.

[5] A. Chomyn, G. Meola, N. Bresolin, et al., In vitro genetic transfer of protein synthesis and respiration defects to mitochondrial DNA-less cells with myopathy-patient mitochondria, Mol. Cell. Biol. 11 (1991) 2236–2244.
[6] M.P. King, Y. Koga, M. Davidson, E.A. Schon, Defects in mitochondrial protein synthesis and respiratory chain activity segregate with the tRNALeu(UUR) mutation associated with mitochondrial myopathy encephalopathy, lactic acidosis, and strokelike episodes, Mol. Cell. Biol. 12 (1992) 480–490.
[7] K. Inoue, K. Nakada, A. Ogura, et al., Generation of mice with mitochondrial dysfunction by introducing mouse mtDNA carrying a deletion into zygotes, Nat. Genet. 26 (2000) 176–181.
[8] K. Nakada, K. Inoue, T. Ono, et al., Inter-mitochondrial complementation: mitochondria-specific system preventing mice from expression of disease phenotypes by mutant mtDNA, Nat. Med. 7 (2001) 934–940.
[9] A. Kasahara, K. Ishikawa, M. Yamaoka, et al., Generation of trans-mitochondrial mice carrying homoplasmic mtDNAs with a missense mutation in a structural gene using ES cells, Hum. Mol. Genet. 15 (2006) 871–881.
[10] M. Yokota, H. Shitara, O. Hashizume, et al., Generation of trans-mitochondrial mito-mice by the introduction of a pathogenic G13997A mtDNA from highly metastatic lung carcinoma cells, FEBS Lett. 584 (2010) 3943–3948.
[11] O. Hashizume, A. Shimizu, M. Yokota, et al., Specific mitochondrial DNA mutation in mice regulate diabetes and lymphoma development, Proc. Natl. Acad. Sci. U. S. A. 109 (2012) 10528–10533.
[12] A. Shimizu, T. Mito, C. Hayashi, et al., Transmitochondrial mice as models for primary prevention of diseases caused by mutation in the *tRNA^{Lys}* gene, Proc. Natl. Acad. Sci. U. S. A. 111 (2014) 3104–3109.
[13] M. Houshmand, C. Lindberg, A.R. Moslemi, et al., A novel hetero-plasmic point mutation in the mitochondrial tRNA(Lys) gene in a sporadic case of mitochondrial encephalomyopathy: De novo mutation and no transmission to the offspring, Hum. Mutat. 13 (1999) 203–209.
[14] E.L. Blakely, H. Swalwell, R.K. Petty, et al., Sporadic myopathy and exercise intolerance associated with the mitochondrial 8328G>A tRNA^{Lys} mutation, J. Neurol. 254 (2007) 1283–1285.
[15] J. Wang, H. Wilhelmsson, C. Graff, et al., Dilated cardiomyopathy and atrioventricular conduction blocks induced by heart-specific inactivation of mitochondrial DNA gene expression, Nat. Genet. 21 (1999) 133–137.
[16] A. Nedergaard, K. Henriksen, M.A. Karsdal, C. Christiansen, Musculoskeletal ageing and primary prevention, Best. Pract. Res. Clin. Obstet. Gynaecol. 27 (2013) 673–688.
[17] B.H. Cohen, Neuromuscular and systemic presentations in adults: diagnoses beyond MERRF and MELAS, Neurotherapeutics 10 (2013) 227–242.
[18] A. Trifunovic, A. Wredenberg, M. Falkenberg, et al., Premature ageing in mice expressing defective mitochondrial DNA polymerase, Nature 429 (2004) 417–423.
[19] G.C. Kujoth, A. Hiona, T.D. Pugh, et al., Mitochondrial DNA mutations, oxidative stress, and apoptosis in mammalian aging, Science 309 (2005) 481–484.
[20] T. Mito, H. Ishizaki, M. Suzuki, et al., Transmitochondrial mito-miceΔ and mtDNA mutator mice, but not aged mice, share the same spectrum of musculoskeletal disorders, Biochem. Biophys. Res. Commun. 456 (2015) 933–937.
[21] A. Rötig, J.L. Bessis, N. Romero, et al., Maternally inherited duplication of the mitochondrial genome in a syndrome of proximal tubulopathy, diabetes mellitus, and cerebellar ataxia, Am. J. Hum. Genet. 50 (1992) 364–370.
[22] J.J. Jansen, J.A. Maassen, F.J. van der Woude, et al., Mutation in mitochondrial tRNA(Leu(UUR)) gene associated with progressive kidney disease, J. Am. Soc. Nephrol. 8 (1997) 1118–1124.
[23] M.J. Szabolcs, R. Seigle, S. Shanske, et al., Mitochondrial DNA deletion: a cause of chronic tubulointerstitial nephropathy, Kidney Int. 45 (1994) 1388–1396.
[24] J.-I. Hayashi, Y. Tagashira, M.C. Yoshida, et al., Two distinct types of mitochondrial DNA segregation in mouse-rat hybrid cells: stochastic segregation and chromosome-dependent segregation, Exp. Cell. Res. 147 (1983) 51–61.
[25] J.P. Jenuth, A.C. Peterson, K. Fu, E.A. Shoubridge, Random genetic drift in the female germline explains the rapid segregation of mammalian mitochondrial DNA, Nat. Genet. 14 (1996) 146–151.
[26] C. Freyer, L.M. Cree, A. Mourier, et al., Variation in germline mtDNA heteroplasmy is determined prenatally but modified during subsequent transmission, Nat. Genet. 44 (2012) 1282–1285.
[27] K. Nakada, A. Sato, H. Sone, et al., Accumulation of pathogenic ΔmtDNA induced deafness but not diabetic phenotypes in mito-mice, Biochem. Biophys. Res. Commun. 323 (2004) 175–184.

PLOS | ONE

RESEARCH ARTICLE

A Specific Nuclear DNA Background Is Required for High Frequency Lymphoma Development in Transmitochondrial Mice with G13997A mtDNA

Osamu Hashizume[1☯], Haruka Yamanashi[2☯], Makoto M. Taketo[3], Kazuto Nakada[1,4], Jun-Ichi Hayashi[1,4,5*]

1 Faculty of Life and Environmental Sciences, University of Tsukuba, 1-1-1 Tennodai, Tsukuba, Ibaraki, Japan, **2** Graduate School of Life and Environmental Sciences, University of Tsukuba, 1-1-1 Tennodai, Tsukuba, Ibaraki, Japan, **3** Department of Pharmacology, Graduate School of Medicine, Kyoto University, Yoshida-Konoe-cho, Sakyou-ku, Kyoto, Japan, **4** International Institute for Integrative Sleep Medicine (WPI-IIIS), University of Tsukuba, 1-1-1 Tennodai, Tsukuba, Ibaraki, Japan, **5** TARA center, University of Tsukuba, 1-1-1 Tennodai, Tsukuba, Ibaraki, Japan

☯ These authors contributed equally to this work.
* jih45@biol.tsukuba.ac.jp

Citation: Hashizume O, Yamanashi H, Taketo MM, Nakada K, Hayashi J-I (2015) A Specific Nuclear DNA Background Is Required for High Frequency Lymphoma Development in Transmitochondrial Mice with G13997A mtDNA. PLoS ONE 10(3): e0118561. doi:10.1371/journal.pone.0118561

Academic Editor: Feng Ling, RIKEN Advanced Science Institute, JAPAN

Received: October 27, 2014

Accepted: January 20, 2015

Published: March 4, 2015

Data Availability Statement: All relevant data are within the paper.

Funding: This work was supported by Grants-in-Aid for Scientific Research A 25250011 (to JH), Scientific Research A 23240058 (to KN), and Scientific Research on Innovative Areas 24117503 (to JH) from the Japan Society for the Promotion of Science. This work was supported also by the World Premier International Research Center Initiative; Ministry of Education, Culture, Sports, Science and Technology–Japan (to KN and J-IH). The funders had no role in

Abstract

We previously found that mouse mitochondrial DNA (mtDNA) with a G13997A mutation (G13997A mtDNA) controls not only the transformation of cultured lung carcinoma cells from poorly metastatic into highly metastatic cells, but also the transformation of lymphocytes into lymphomas in living C57BL/6 (B6) mice. Because the nuclear genetic background of the B6 strain makes the strain prone to develop lymphomas, here we examined whether G13997A mtDNA independently induces lymphoma development even in mice with the nuclear genetic background of the A/J strain, which is not prone to develop lymphomas. Our results showed that the B6 nuclear genetic background is required for frequent lymphoma development in mice with G13997A mtDNA. Moreover, G13997A mtDNA in mice did not enhance the malignant transformation of lung adenomas into adenocarcinomas or that of hepatocellular carcinomas from poorly metastatic into highly metastatic carcinomas. Therefore, G13997A mtDNA enhances the frequency of lymphoma development under the abnormalities in the B6 nuclear genome, and does not independently control tumor development and tumor progression.

Introduction

Mitochondrial respiration defects and the resultant enhanced glycolysis under normoxia, that is, the Warburg effect, enable cell growth under hypoxia, and thus are thought to be involved in tumor development [1–4]. Because pathogenic mtDNA mutations also induce mitochondrial respiration defects and the Warburg effect, age-associated accumulation of pathogenic

study design, data collection and analysis, decision to publish, or preparation of the manuscript.

Competing Interests: The authors have declared that no competing interests exist.

mutations in mtDNA and the resultant age-associated expression of mitochondrial respiration defects are considered to be responsible for tumor development [5, 6]. In fact, somatic mutations are preferentially accumulated in tumor mtDNA [7–9].

In contrast, our previous studies provided convincing evidence that mtDNA with a pathogenic G13997A mutation in the ND6 gene (G13997A mtDNA) controls the malignant transformation of carcinoma cells from a poorly metastatic phenotype into a highly metastatic one [10], although mtDNA does not control tumor development (the transformation of normal cells into tumor cells) [10, 11]. Moreover, the induction of high metastasis was not due to respiration defects and the resultant Warburg effect, but to overproduction of reactive oxygen species (ROS) [12].

Subsequently, we generated transmitochondrial mito-mice-ND6^{13997} (B6mtND6^{13997}) carrying the nuclear genome from B6 mice and G13997A mtDNA from highly metastatic carcinoma cells [13], and showed that they developed lymphoma with high frequency [14], indicating the possible involvement of mtDNA mutations in tumor development. However, no tumor development was observed in transmitochondrial mito-mice-COI^{6589} (B6mtCOI^{6589}) with T6589C mtDNA [14]. Because these mice expressed respiration defects and the Warburg effect [15], but did not overproduce ROS, we proposed that ROS overproduction but not the Warburg effect would be responsible for high frequency lymphoma development [14].

These findings raise several questions: Does G13997A mtDNA independently induce lymphomas even in mice with a nuclear genetic background that is not prone to develop lymphomas? Does G13997A mtDNA also induce high metastasis in tumors developed in mice, given that it induces high metastasis in a low metastatic lung carcinoma cell line [10]? To answer these questions, here we generated mice possessing G13997A mtDNA and nuclear genetic background derived from the A/J strain, which is not prone to develop lymphoma [16] and from mice that are prone to develop hepatocellular carcinomas [17, 18]. Moreover, we treated the mice with urethane to enhance lung adenoma development [19, 20], and examined its effects on the malignant transformation of adenomas into adenocarcinomas in mice with G13997A mtDNA.

The results suggest that G13997A mtDNA enhances the frequency of lymphoma development that is primarily caused by abnormalities in the B6 nuclear genome. Moreover, it does not always enhance transformation of normal cells in mice or malignant transformation of tumor cells developed in mice, probably due to the requirement of some nuclear abnormalities.

Materials and Methods

Ethics statement

All animal experiments were performed in accordance with protocols approved by the Institutional Animal Care and Use Committee of University of Tsukuba, Japan (Permit Number: 12-264, 13-312, and 14-271).

Mice

B6 mice were purchased from CLEA Japan (Tokyo, Japan), and A/J mice were purchased from Japan SLC (Shizuoka, Japan). Mito-miceND6^{13997} (B6mtND6^{13997} mice) were generated previously [13]. Lkb1 (+/−) mice were obtained from Kyoto University. Female B6 and B6mtND6^{13997} mice were crossed with B6, A/J and Lkb1 (+/−) males. F_1 males obtained from the cross between B6 or B6mtND6^{13997} females with A/J males were used for urethane treatment experiments. F_1 females obtained from the cross between B6 females or B6mtND6^{13997} females with A/J males were furthermore backcrossed to A/J males to obtain F_2 and F_3 generations. F_3 males were used to study the spontaneous lung tumor formation. Mice were

monitored every day for general health, and those with signs of tumor burden, such as hunched posture, ruffled coats, and respiratory distress, were euthanized by cervical dislocation. The maximum tumor size (diameter) was less than 7 mm in sacrificed mice. When mice were sacrificed, anesthesia with an intraperitoneal injection of 2.5% avertin was employed to minimize animal suffering. All mice were maintained on hardwood bedding on a 12-h light/dark cycle and given food and water ad libitum.

Measurement of ROS production in mitochondria

ROS generation was detected with the mitochondrial superoxide indicator MitoSOX-Red (Invitrogen, Carlsbad, CA, USA). 1×10^5 cells were incubated with 1 mM MitoSOX-Red for 15 min at 37°C in phosphate-buffered saline (PBS), washed twice with PBS, and then immediately analyzed with a FACScan flow cytometer (Becton Dickinson, San Jose, CA, USA). Data were analyzed with FlowJo software (Tree Star, USA). Relative ROS levels were calculated as mean fluorescence intensity of MitoSOX-Red stained cells minus autofluorescence of the unstained cells.

Urethane treatment

B6 strain mice were injected intraperitoneally (IP) at 4 weeks of age with 1 mg/g body weight urethane (ethyl carbamate; SIGMA, St. Louis, MO, USA) weekly for a total of 10 doses. Groups of F_1 hybrid mice were injected IP at 4 weeks of age with 1 mg/g body weight urethane weekly for a total of 2 doses. Tumor multiplicities were examined 52 weeks after the initial urethane injection.

Histological analyses

Lungs and livers were fixed in formalin solution. Tumors greater than 0.5mm in diameter on the lung surface were counted after fixation. After overnight fixation in 10% buffered formalin, tissues were paraffin embedded, cut into 8-μm sections, placed on glass slides, and stained with hematoxylin and eosin. Formalin-fixed, paraffin-embedded serial sections were used for histological analysis.

Statistical analysis

We analyzed data with the (unpaired or paired) Student t-test. Kaplan–Meier curves were assessed with the log-rank test. Values with $P < 0.05$ were considered significant.

Results

Generation of A/J mice with G13997A mtDNA (A/JmtND6^{13997}) by backcrossing

First, we asked whether B6 mtDNA with the G13997A mutation (G13997A mtDNA) in B6mtND6^{13997} mice independently regulates lymphoma development. To answer this question, we needed to generate A/JmtND6^{13997} mice carrying G13997A mtDNA in the nuclear genetic background of the A/J strain, which is not predisposed to developing lymphoma [16].

To generate A/JmtND6^{13997} mice, an F_1 female obtained by mating a B6mtND6^{13997} female with an A/J male was backcrossed to an A/J male, and the resultant F_2 females were further backcrossed to A/J males, resulting in the generation of F_3 mice (A/JmtND6^{13997}). A/JmtND6^{13997} mice thus carry a nuclear genetic background derived mostly from the A/J strain and possess only G13997A mtDNA (Table 1). As a negative control, we generated F_3 A/JmtB6 mice carrying B6 mtDNA without the G13997A mutation with a nuclear genetic background

Table 1. Effects of nuclear-background variations and the presence or absence of B6-derived mtDNA with the G13997A mutation on the tumor-related phenotypes of mice.

Mice	Strains		No. of mice	Urethane treatment*	No. of mice with tumors / no. of mice examined				
	nuclear DNA	mtDNA			Lymphoma	Pulmonary nodules (No. of nodules)	Liver carcinomas	Lung metastasis (No. of nodules)	others
B6	B6	B6	35	–	3/35**	0/35**	0/35**	0/35**	0/35**
B6mtND6^{13997}	B6	B6 (G13997A)	35	–	16/35**	0/35**	0/35**	0/35**	0/35**
A/JmtB6	A/J	B6	5	–	0/5	4/5 (3.75 ± 0.5)	0/5	0/5	0/5
A/JmtND6^{13997}	A/J	B6 (G13997A)	6	–	0/6	5/6 (3.2 ± 1.5)	0/6	0/6	0/6
B6	B6	B6	10	++	0/10***	10/10 (8.0 ± 9.7)	0/10	0/10	0/10
B6mtND6^{13997}	B6	B6 (G13997A)	12	++	0/12***	12/12 (7.83 ± 6.5)	0/12	0/12	0/12
B6 × A/J (F_1)	B6 × A/J	B6	6	+	0/6	6/6 (17.3 ± 3.9)	0/6	0/6	0/6
B6mtND6^{13997} × A/J (F_1)	B6 × A/J	B6 (G13997A)	5	+	0/5	5/5 (21.6 ± 8.0)	0/5	0/5	0/5
Lkb1 (+/–)	B6 (Lkb1+/–)	B6	19	–	0/19****	0/19	14/19	2/14 (2.5 ± 0.7)	0/19
Lkb1 (+/–) mtND6^{13997}	B6 (Lkb1+/–)	B6 (G13997A)	16	–	0/16****	0/16	13/16	2/13 (2 ± 0)	0/16

* B6 mice and B6mtND6^{13997} mice sharing the B6 nuclear genetic background received weekly urethane administration for 10 times (++). In contrast, F_1 hybrids between B6 females and A/J males and F_1 hybrids between B6mtND6^{13997} females and A/J males received weekly administration of urethane for only twice (+) due to their higher susceptibility to urethane treatment than mice with B6 nuclear genetics background.

** These results were reported previously (Hashizume et al., 2012).

*** No mice developed lymphoma, since they were sacrificed to detect lung adenoma at 12 months of age.

**** No mice developed lymphoma, since they died due to the Lkb1 mutation before lymphoma development.

doi:10.1371/journal.pone.0118561.t001

derived mostly from the A/J strain. A/JmtND6^{13997} mice and A/JmtB6 mice thus share the nuclear and mitochondrial genetic backgrounds except that A/JmtND6^{13997} mice carry the G13997A mutation in mtDNA (Table 1).

Examination of tumor formation in A/JmtND6^{13997} mice

Five A/JmtB6 males and six A/JmtND6^{13997} males were available to investigate the effects of the A/J nuclear genetic background on lifespan and the spectrum of tumor formation. Median survival times of A/JmtB6 and A/JmtND6^{13997} mice were 25.0 months and 22.0 months, respectively (Fig. 1), and were similar to those observed in B6 mice (26.1 months) and B6mtND6^{13997} mice (24.6 months) with the B6 nuclear genetic background [14]. Thus, the lifespans were not affected by the presence or absence of the G13997A mutation or by the difference in the nuclear genetic backgrounds.

Gross necropsy of all euthanized moribund A/JmtB6 mice and A/JmtND6^{13997} mice showed that no mice developed lymphomas or other tumors except pulmonary nodules, irrespective of whether they possessed the G13997A mutation (Table 1). Given that the nuclear genetic background of the A/J strain is not prone to develop lymphoma, these data indicate that the B6 nuclear genetic background, which predisposes mice to develop lymphoma [16, 21–23], is required to induce high frequency lymphoma development in B6mtND6^{13997} mice [14]. Moreover, the G13997A mutation in mtDNA does not independently induce lymphoma development. Thus, G13997A mtDNA simply enhances the lymphoma-prone phenotype that is regulated by the B6 strain-derived nuclear genome. To confirm this idea, larger studies using

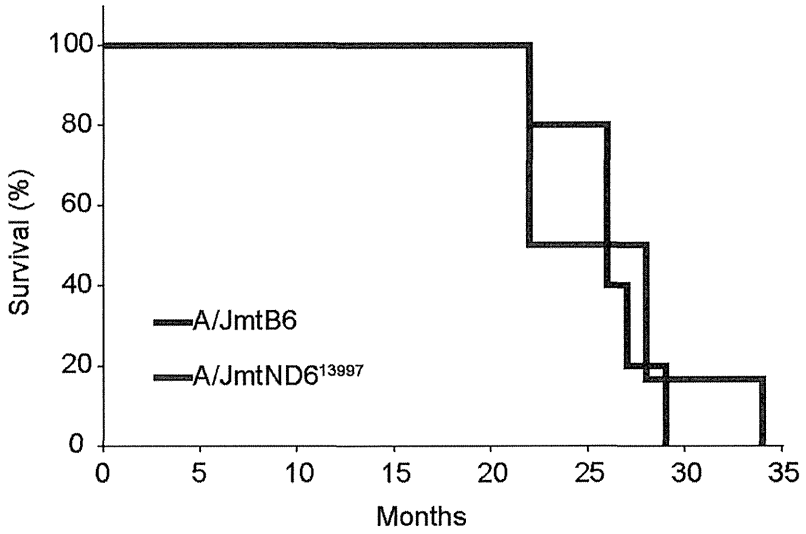

Fig 1. Kaplan-Meier survival curves of A/JmtB6 and A/JmtND6^{13997} mice. Median survival times of A/JmtB6 mice (n = 5) and A/JmtND6^{13997} mice (n = 6) were 25.0 months and 22.0 months, respectively. No statistically significant differences in median survival times were observed (p = 0.2216).

doi:10.1371/journal.pone.0118561.g001

more animals than were used in this study are required, because we were unable to exclude the possibility that there was a low level of lymphoma formation in F_3 mice with the A/J nuclear background.

We then compared ROS levels in bone marrow cells of A/JmtB6 (18-month-old male) and A/JmtND6^{13997} (18-month-old male) mice, using age-matched B6 males and B6mtND6^{13997} males as controls (Fig. 2A). A/JmtND6^{13997} mice did not show ROS overproduction (Fig. 2B), indicating that the A/J nuclear background might possess systems to suppress ROS overproduction by G13997A mtDNA. In contrast, ROS levels of B6 mice and A/JmtB6 mice were similar (Fig. 2B), indicating that suppression of lymphoma development in A/J mice but not in B6 mice was due to some nuclear factors in A/J mice that suppress signals of lymphoma development.

The mice with the A/J nuclear genetic background frequently developed pulmonary nodules (Table 1). The results were expected, because A/J mice are known to develop lung adenomas [16]. However, the numbers of pulmonary nodules did not differ substantially between A/JmtB6 mice and A/JmtND6^{13997} mice (Table 1). Our histological analysis of the pulmonary nodules suggested that they were all lung adenomas (Fig. 3). These observations indicate that the G13997A mutation in mtDNA does not enhance either the number of lung adenomas or the malignant progression of lung adenomas into lung adenocarcinomas in mice with the A/J nuclear genetic background.

Effects of G13997A mtDNA on malignant progression of urethane-induced adenomas

To further assess whether G13997A mtDNA enhances the malignant progression of lung adenomas into adenocarcinomas, we treated the mice with urethane to induce early onset and enhance the frequency of lung adenoma development. Because F_1 hybrids between B6 and A/J mice are more susceptible to lung adenoma development than are B6 mice [19], we used six F_1 hybrids between B6 females and A/J males and five F_1 hybrids between B6mtND6^{13997} females and A/J males. We also used ten B6 mice and twelve B6mtND6^{13997} mice.

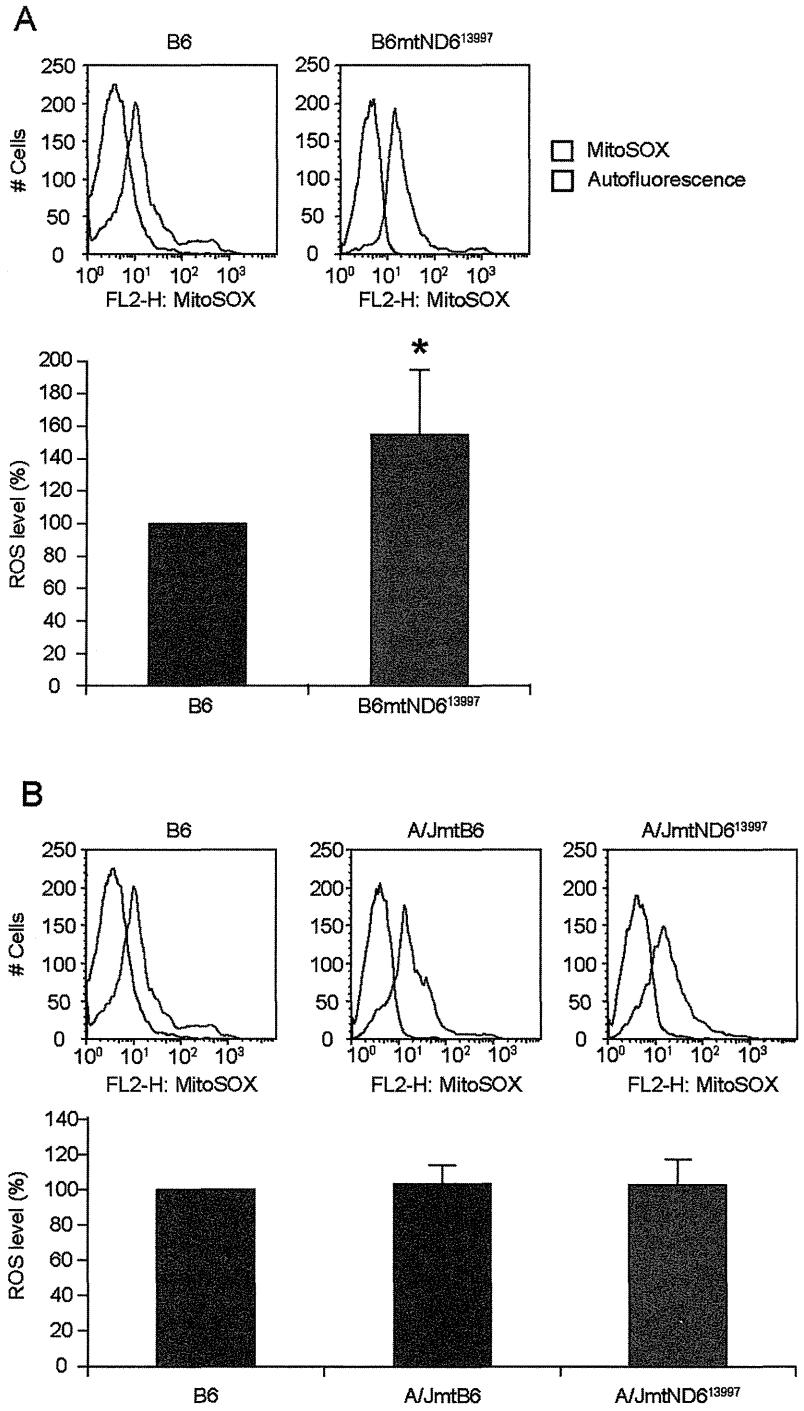

Fig 2. Estimation of mitochondrial superoxide (i.e., reactive oxygen species, ROS) levels in bone marrow cells after treatment with MitoSOX-Red. (A) ROS levels in bone marrow cells from mice with B6 nuclear background. (B) ROS levels in bone marrow cells from mice with A/J nuclear background. B6 mice were used as controls. Upper panels, representative flow cytometry histograms of MitoSOX-Red. Lower panels, relative ROS levels calculated by FlowJO as mean fluorescence intensity for MitoSOX-Red minus background autofluorescence of the unstained cells. Data are presented as mean values with SD (n = 3). *$P < 0.05$ compared with control B6 mice.

doi:10.1371/journal.pone.0118561.g002

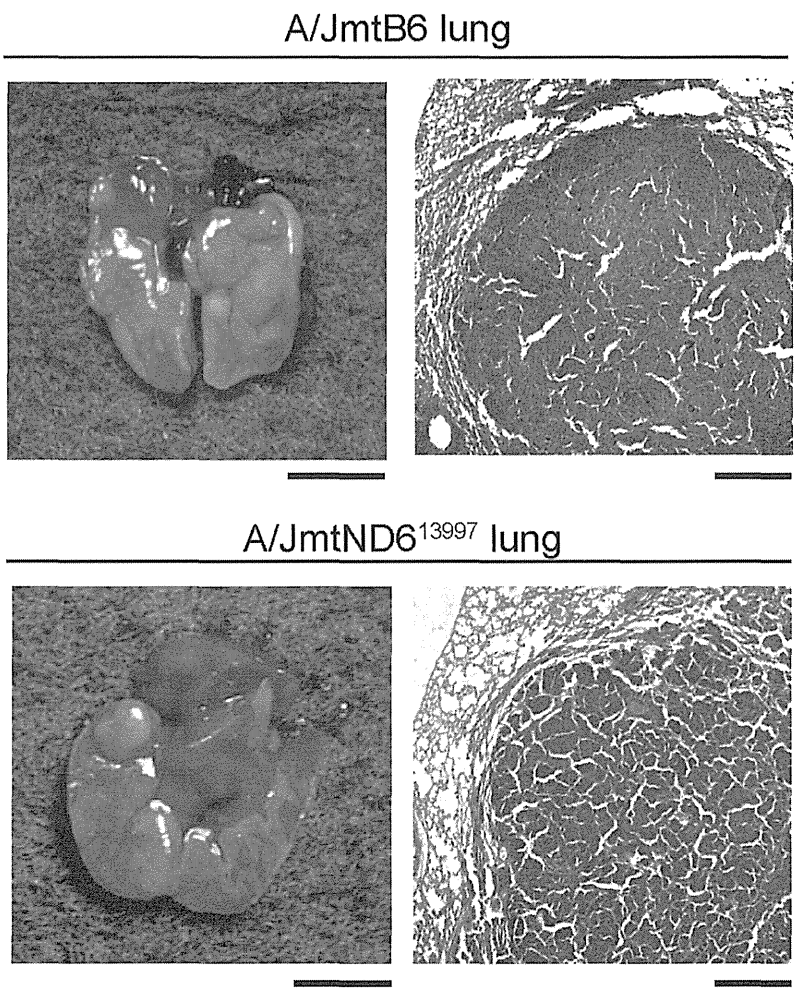

Fig 3. Lung adenoma formation in A/JmtB6 and A/JmtND6^{13997} mice. Gross necropsy (left) and hematoxylin and eosin staining of histological sections (right) of the lung. Most mice with the A/J nuclear genetic background developed lung adenomas. The frequencies of lung adenoma formation in A/JmtB6 and A/JmtND6^{13997} mice were 80% (4/5) and 83.3% (5/6), respectively. Scale bars: left, 5 mm; right, 200 μm.

doi:10.1371/journal.pone.0118561.g003

Based on urethane-administration protocols [19, 20], B6 mice and B6mtND6^{13997} mice, which share the same B6 nuclear genetic background received 10 weekly urethane injections beginning 4 weeks after birth. In contrast, F_1 hybrids between B6 females and A/J males and F_1 hybrids between B6mtND6^{13997} females and A/J males received only 2 weekly injections of urethane due to their higher susceptibility to urethane treatment than that of mice with the B6 nuclear genetic background.

The urethane-treated mice were examined one year after the birth. All of the mice developed pulmonary nodules, but the F_1 hybrids had more pulmonary nodules than did mice with the B6 nuclear genetic background, even though the latter mice received more urethane treatments (Table 1). There was no noteworthy difference in nodule numbers between the B6 and B6mtND6^{13997} mice or between the F_1 hybrids with or without the G13997A mutation in their mtDNA (Table 1).

Histological analysis of the pulmonary nodules (Fig. 4) showed that they were all lung adenomas: malignant progression to adenocarcinomas was not observed even in mice possessing G13997A mtDNA (B6mtND6^{13997} mice and F_1 hybrids between B6mtND6^{13997} females and A/J males). These results demonstrate that G13997A mtDNA does not induce the tumor

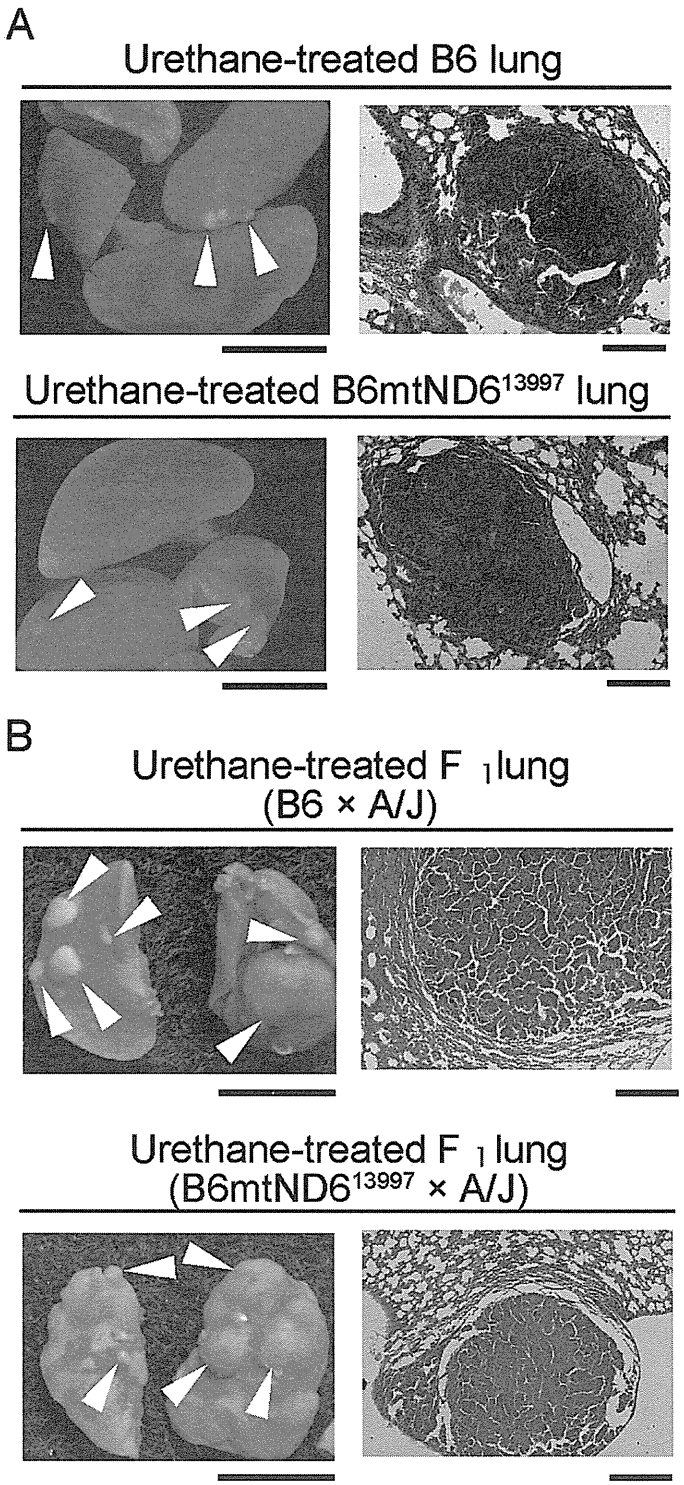

Fig 4. Enhanced development of lung adenomas after urethane administration. Urethane-treated mice with the nuclear genetic background of B6 (A) and of F_1 hybrids between B6 and A/J mice (B). Gross necropsy of formalin-fixed lungs (left), which were sectioned and stained with hematoxylin and eosin (right). Small tumors (indicated by arrowheads) were observed on the surface of the lungs. Histological analysis showed that these tumor-like abnormalities corresponded to adenomas. The numbers of lung tumors that developed in B6, in B6mtND6^{13997}, and in F_1 hybrids between B6 females × A/J males and between B6mtND6^{13997} females × A/J males were 8.0 ± 9.7, 7.8 ± 6.5, 17.3 ± 3.9 and 21.6 ± 8.0, respectively. Scale bars: (A) left, 5mm; right, 100μm, (B) left, 5mm; right, 200μm.

doi:10.1371/journal.pone.0118561.g004

progression of lung adenomas into adenocarcinomas, even when the early onset and frequency of adenoma development are enhanced by urethane administration.

Effects of G13997A mtDNA on the metastasis of hepatocellular carcinomas in Lkb1 (+/–) mice

Finally, we investigated whether G13997A mtDNA enhances metastasis in mice with a nuclear abnormality that induces the development of metastasis-prone carcinomas. To this end, we used Lkb1 (+/–) mice with the B6 nuclear genetic background to introduce G13997A mtDNA. The Lkb1 gene is a tumor suppressor gene that plays a role in cell cycle arrest and apoptosis [17]. Most Lkb1 (+/–) mice develop hepatocellular carcinomas within 40 weeks of birth; 10% of them subsequently form lung metastases in the ensuing 10 weeks [18]. Our previous studies showed that G13997A mtDNA is responsible for the high frequency of lymphoma development in lymphoma-prone B6 mice [14] and for the high frequency of lung metastasis in metastasis-prone lung carcinoma cells [10]. Therefore, we expected that G13997A mtDNA would also induce a high frequency of lung metastasis in metastasis-prone Lkb1 (+/–) mice [18].

First, we mated B6mtND6^{13997} females to Lkb1 (+/–) males, and obtained F_1 Lkb1 (+/–) mice possessing G13997A mtDNA (Lkb1 (+/–) mtND6^{13997}). Then, we monitored 19 male Lkb1 (+/–) mice and 16 male Lkb1 (+/–) mtND6^{13997} mice for signs of tumor formation. The median survival times for the Lkb1 (+/–) mice and Lkb1 (+/–) mtND6^{13997} mice were 14.1 and 14.0 months, respectively, and no statistically significant differences were observed between them (Fig. 5).

Gross necropsy of all of the euthanized moribund mice showed that 14 of the 19 Lkb1 (+/–) mice and 13 of the 16 Lkb1 (+/–) mtND6^{13997} mice developed tumor-like abnormalities in the liver (Table 1). Histological analysis of the liver abnormalities revealed that all of these tumor-like abnormalities were hepatocellular carcinomas (Fig. 6A). Moreover, two of the 14 Lkb1 (+/–) mice and two of the 13 Lkb1 (+/–) mtND6^{13997} mice that developed hepatocellular carcinomas had 2–3 lung nodules (Table 1, Fig. 6B). Therefore, the frequencies of lung metastasis did not change substantially in Lkb1 (+/–) mtND6^{13997} mice, indicating that the G13997A mutation in mtDNA did not enhance lung metastasis in Lkb1 (+/–) mice.

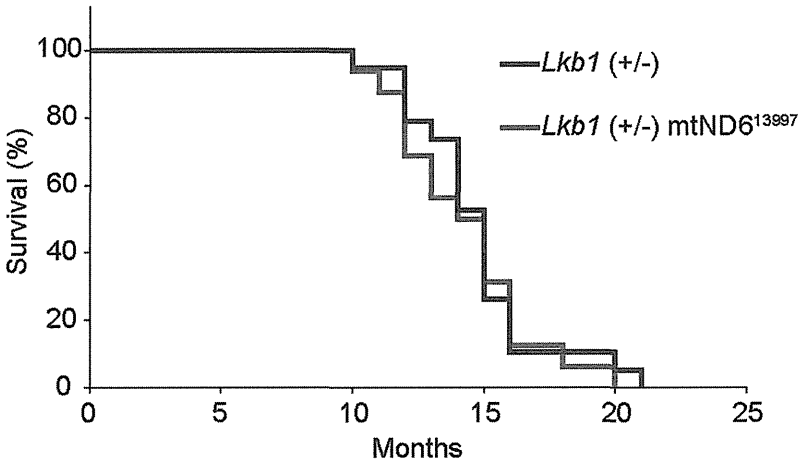

Fig 5. Kaplan-Meier survival curves of Lkb1 (+/–) and Lkb1 (+/–) mtND6^{13997} mice. Median survival times of Lkb1 (+/–) (n = 19) and Lkb1 (+/–) mtND6^{13997} mice (n = 16) were 14.1 months and 14.0 months, respectively. No statistically significant differences in median survival times were observed between them (p = 0.1892).

doi:10.1371/journal.pone.0118561.g005

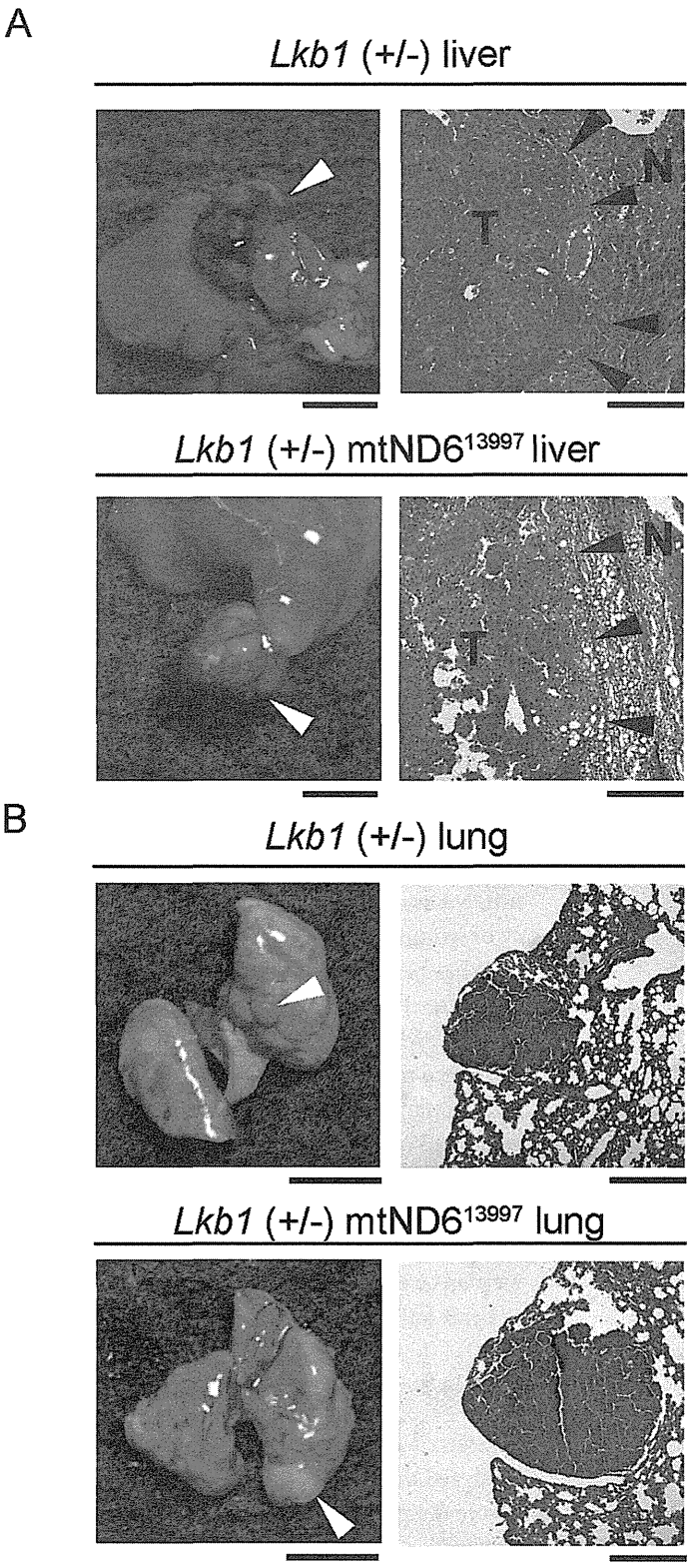

Fig 6. Development of tumors in the liver and metastatic nodules in the lungs of Lkb1 (+/–) and Lkb1 (+/–) mtND6^{13997} mice. Gross necropsy (left) and histological sections (right) of livers (A) and lungs (B). White arrowheads indicate hepatocellular carcinomas in the liver (A) and metastatic nodules in the lung (B). Black arrowheads on the liver sections (A) indicate the borders between the developed tumors (T) and the